Hindawi
Shock and Vibration
Volume 2017, Article ID 7687802, 12 pages
https://doi.org/10.1155/2017/7687802

Research Article

Dynamic Fracturing Behavior of Layered Rock with Different Inclination Angles in SHPB Tests

Jiadong Qiu, Diyuan Li, Xibing Li, and Zilong Zhou

School of Resources and Safety Engineering, Central South University, Changsha 410083, China

Correspondence should be addressed to Diyuan Li; diyuan.li@csu.edu.cn

Received 11 June 2017; Accepted 12 October 2017; Published 12 December 2017

Academic Editor: Salvatore Russo

The fracturing behavior of layered rocks is usually influenced by bedding planes. In this paper, five groups of bedded sandstones with different bedding inclination angles θ are used to carry out impact compression tests by split Hopkinson pressure bar. A high-speed camera is used to capture the fracturing process of specimens. Based on testing results, three failure patterns are identified and classified, including (A) splitting along bedding planes; (B) sliding failure along bedding planes; (C) fracturing across bedding planes. The failure pattern (C) can be further classified into three subcategories: (C1) fracturing oblique to loading direction; (C2) fracturing parallel to loading direction; (C3) mixed fracturing across bedding planes. Meanwhile, a numerical model of layered rock and SHPB system are established by particle flow code (PFC). The numerical results show that the shear stress is the main reason for inducing the damage along bedding plane at $\theta = 0^\circ$~75°. Both tensile stress and shear stress on bedding planes contribute to the splitting failure along bedding planes when the inclination angle is 90°. Besides, tensile stress is the main reason that leads to the damage in rock matrixes at $\theta = 0^\circ$~90°.

1. Introduction

Transversely isotropic rock is widely encountered in rock mechanics and rock engineering. Many sedimentary rocks and some metamorphic rocks, such as slate, shale, gneiss, and sandstone, belong to transversely isotropic rocks. Generally, the mechanical behaviors of these rocks are highly related to the orientation of bedding planes, exhibiting strong strength anisotropy and deformation anisotropy [1–5]. Several types of rocks with bedding planes (e.g., slate, shale, sandstone, and coal) tend to split or break along the bedding planes rather than in other orientations.

The research on the mechanical properties of transversely isotropic rocks has attracted the attention of many scholars. The single weakness plane theory proposed by Jaeger [6, 7] is the first attempt to describe the strength anisotropy of transversely isotropic rock. In this theory, the failure behaviors are classified into two independent modes, including failure along the discontinuity and failure through intact rock. Xian and Tan [8] have carried out a theoretical investigation on the layered rock masses under static loading, indicating that the bedding plane and filling materials have straightforward effects on the failure mechanism. Ramamurthy et al. [9] have investigated the anisotropy of phyllites and proposed a strength criterion to predict nonlinear strength behavior of transversely isotropic rocks. Tien and Kuo [4] have modified Jaeger's criterion and the Hoek-Brown criterion to accommodate two different failure modes (a sliding mode along the discontinuity and a nonsliding failure mode) for transversely isotropic rocks. Saeidi et al. [10] have also modified the Hoek-Brown criterion and Ramamurthy criterion to predict the strength of transversely isotropic rock under triaxial loading condition. Both of them have found that the strength of transverse isotropic rocks exhibit a U-shaped trend with the inclination angle increasing under static loading conditions [10, 11]. For numerical simulation, Dan and Konietzky [12] have found that the failure patterns of transverse isotropic rocks can be classified into three types (pure tensile failure, matrix-bedding tensile-shear failure, and bedding tensile-shear failure) with foliation-loading angle varying. By using the discrete element method, Tan et al. [13] have drew a diagram which reflects the relationship between tensile strength, failure patterns, and foliation-loading angle of transverse isotropic rocks.

As mentioned above, the failure patterns and the strength of transversely isotropic rocks under static loading condition will be affected by the inclination angle. However, under dynamic loading condition, the effects of inclination angle on transversely isotropic rock have been paid less attention. Compared with static loading, the mechanical behavior of layered rocks is more complex under dynamic loading. The dynamic strength of rocks shows obvious strain rate effect [14]. Engineering practices also indicate that shock wave caused by earthquake or blasting excavation is an important factor for rock damage and rock failure [15]. Therefore, the researches on the dynamic behavior of transversely isotropic rock are important and necessary. In the theory of stress wave propagation, Li et al. [16] have proposed an equivalent viscoelastic medium method to investigate stress wave propagating across layered rock masses, and they found that the incident angle and the thickness of layered rock mass can affect wave propagation properties. Zhu and Zhao [17] have used virtual wave source method to analyze the obliquely incident stress wave propagating across rock joints and have observed that the amplitude of superposed transmitted wave increases with increasing the incident angel of P-wave.

In dynamic experimental study, Liu et al. [18] have found that the energy consumption for vertical bedded coal-rock is greater than that of the parallel coal at the same fractal dimension. Li et al. [19] have found that Young's modulus of nonpenetrating fractured rock increases with inclination angle increasing. Jia and Zhu [20] have also observed the effects of joint dip angle on the occurrence locations of rock burst. Therefore, the effect of bedding planes on dynamic properties of transversely isotropic rocks is worth studying.

In order to further explore the influence of bedding planes on dynamic compressive fracturing behavior, different inclination angles of sandstone bedding planes have been considered. In tests, five groups of sandstones with different bedding inclination angles 0°, 15°, 45°, 75°, and 90° have been prepared to be tested for bedded sandstones under impact load by split Hopkinson pressure bar (SHPB). Besides, the discrete element method is a good mean to study the fracturing behavior of rock. Through the discrete element method, many scholars have reproduced the fracturing behavior of rock material observed in laboratory and have also investigated the failure evolution [21, 22]. Therefore, the numerical mode with different inclination angle would be established by PFC2D to analyze the micro fracturing mechanism.

2. Experiment

2.1. Testing Equipment. A modified SHPB system is used to carry out the dynamic experiments, as described by Li et al. [23]. The diameter of the incident and transmitted bars is 50 mm. The bars are made of 40Cr alloy steel, with a density of 7.810 g/cm^3, a P-wave velocity of 5400 m/s, and Young's modulus of 240 GPa. The striker is a specific spindle punch, which can generate a half sine wave. This waveform has enough load rising edge so that it can effectively avoid the stress uneven prior to failure [14, 24]. Strain gauges are pasted on the incident and transmitted bars to measure the strains when stress waves spread along elastic bars. Simultaneously, the oscilloscope and data acquisition system capture the signals of strain. In order to observe the fracture development during the impact test, a high-speed camera is used to synchronously capture the failure process of specimens. The frame rate is set to 100000 fps, which means that it can take a picture every 10 μs. The dynamic fracturing process of the bedded sandstone can be recorded by the high-speed camera.

2.2. Specimen Preparation. A yellow sandstone block containing even-spaced bedding planes is selected to prepare the specimens for SHPB test. The yellow sandstone block is obtained from Jiujiang, Jiangxi province, China. Cylindrical specimens are prepared with a nominal diameter of 50 mm and a height of 50 mm. Five different bedding inclination angles θ (the angle between the normal direction of bedding surface and the impact loading direction, as shown in Figure 1) are prepared, including 0°, 15°, 45°, 75°, and 90°. Each group contains at least seven specimens. The specimens are numbered as θ-x where θ means the inclination angle of the bedding planes and x means the number of specimens. Typical bedded sandstone specimens with different inclination angles are shown in Figure 1. It can be seen that the bedding planes are parallel to each other, and the bedding colors alternate between light and dark. As shown in Figure 1, the two mutually perpendicular solid lines marked on the specimen represent the inclination line and the normal line of bedding planes, respectively, where the longer one is the inclination line and the shorter one is the normal line. The dotted line in these figures represents the impact loading direction.

3. Testing Results and Discussion

3.1. Identification of Macro Failure Patterns. According to the fracture development paths and the geometric relationship between main fractures and layer planes, the macro failure pattern can be classified into three types: (A) splitting along bedding planes; (B) sliding along bedding planes; (C) fracturing across bedding planes. The typical pattern of the specimens are shown in detail in Figure 2. The characteristics of the fracturing behavior of the five failure patterns are described as follows.

(A) Splitting along Bedding Planes. This pattern generates the macro main fractures which separate rock specimens along bedding planes. Commonly, these fractures are clean and smooth. Most fractures are parallel to the loading direction, showing the properties of splitting failure. In a few cases, some short branching fractures which are oblique to the loading direction may occur at the tips of main fractures.

(B) Sliding along Bedding Planes. The fractures along bedding planes which are oblique to the loading direction are the main fractures for this pattern. In most cases, the macro fractures directly go through the ends of specimens, and the rock specimens slide along the main fractures. In a few cases, a V-shaped failure zone occurs at the end of rock specimen due to the generation of a new oblique crack, which has different direction with bedding planes.

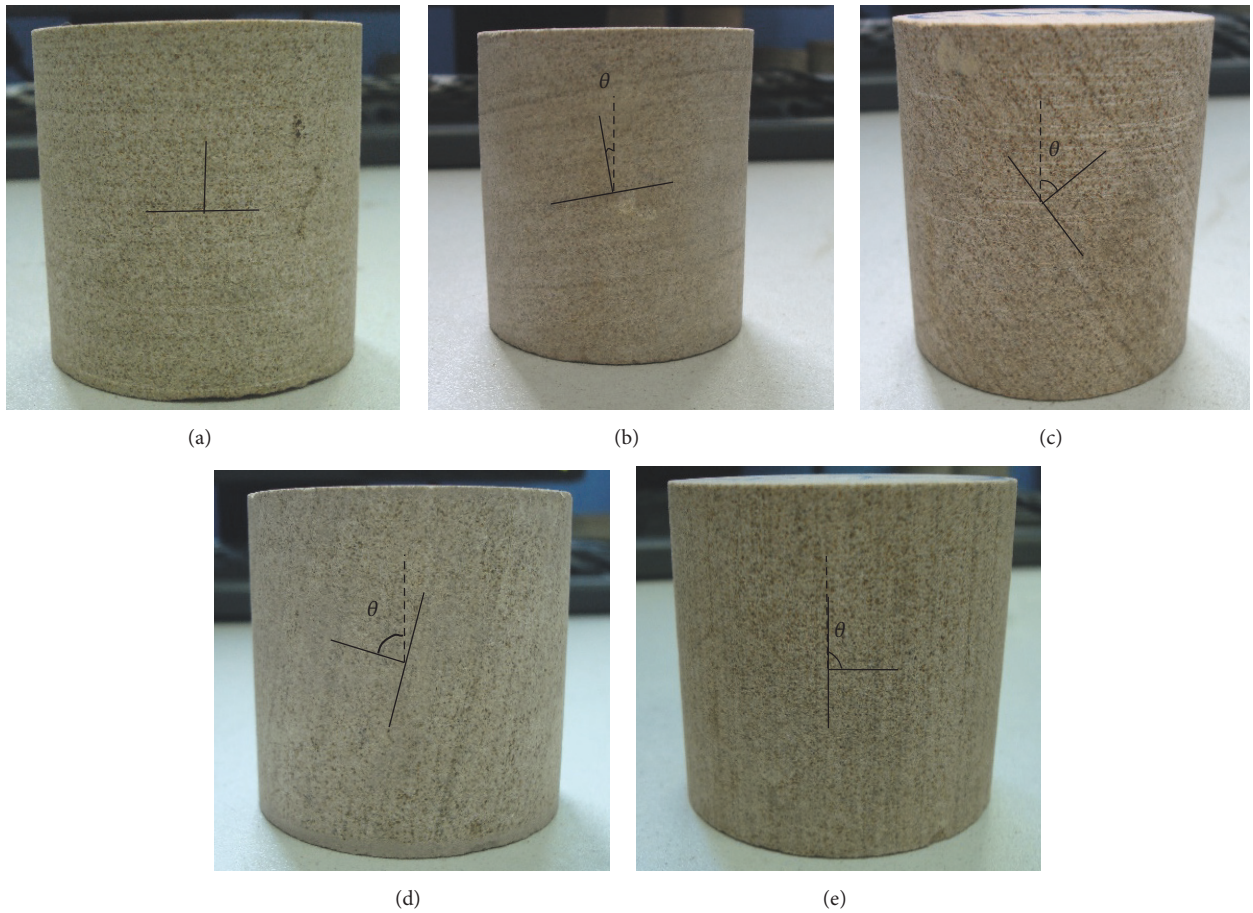

Figure 1: Typical bedded sandstone specimens with different inclination angles ((a) 0-1; (b) 15-2; (c) 45-1; (d) 75-2; (e) 90-2).

(C) Fracturing across Bedding Planes. For this pattern, the macro main fractures penetrate the bedding planes and the failure mainly occurs in rock matrix. In general, the macro main fracture may be oblique to the loading direction or parallel to loading direction. According to the geometric relationship between main fractures and the loading direction, the fracturing across bedding planes can also be classified into three subcategories including (C1) fracturing oblique to loading direction; (C2) fracturing parallel to loading direction; (C3) mixed fracturing across bedding planes.

For the subfailure pattern (C1), the oblique fractures dominate the failure process. The surfaces of main fractures are relatively rough and many tiny dislocations have developed, as shown in Figure 2(C1).

For the specimens with the failure pattern (C2), they have obvious splitting fractures across bedding planes. The splitting fractures paralleled to loading direction are the main macro fractures. Figure 2(C2) shows the typical fracturing process under impact loading. From these pictures, it can be found that the specimen initially generates two splitting fractures across bedding plane at 100 μs. Afterwards, macro failure occurs at about 160 μs.

For the failure pattern (C3), the main fracture may be divided into two parts: the cracks parallel to loading direction and the cracks oblique to loading direction, as shown in Figure 2(C3).

3.2. Effect of Inclination Angle on Failure Patterns. The occurrence ratio of each failure pattern seems to be related to the bedding inclination angles. Figure 3 shows the relationship between failure patterns ratio and the inclination angles. It can be seen that the failure pattern (C1) only is generated at $\theta = 45^\circ$ for all specimens, and similar phenomenon also occurs at $\theta = 0^\circ$ and 75°.

As shown in Figure 3, fracturing across bedding planes is more likely to occur under a lower inclination angle. For example, almost all the specimens of $\theta = 0^\circ \sim 45^\circ$ appear to be fracturing across bedding planes. However, when the inclination angle increases to a certain degree such as 75°, bedding planes will significantly affect the fracturing process and the specimens tend to break along bedding planes.

In conclusion, the variation of the failure pattern with inclination angle has three characteristics. (1) For a low inclination angle (less than 45°), fracturing across bedding planes is the main failure pattern. With the increase of inclination angle, failure pattern (C2) will gradually convert into pattern (C1). (2) For a medium inclination angle (45°–75°), the failure pattern will transform from pattern (C1) to pattern B with

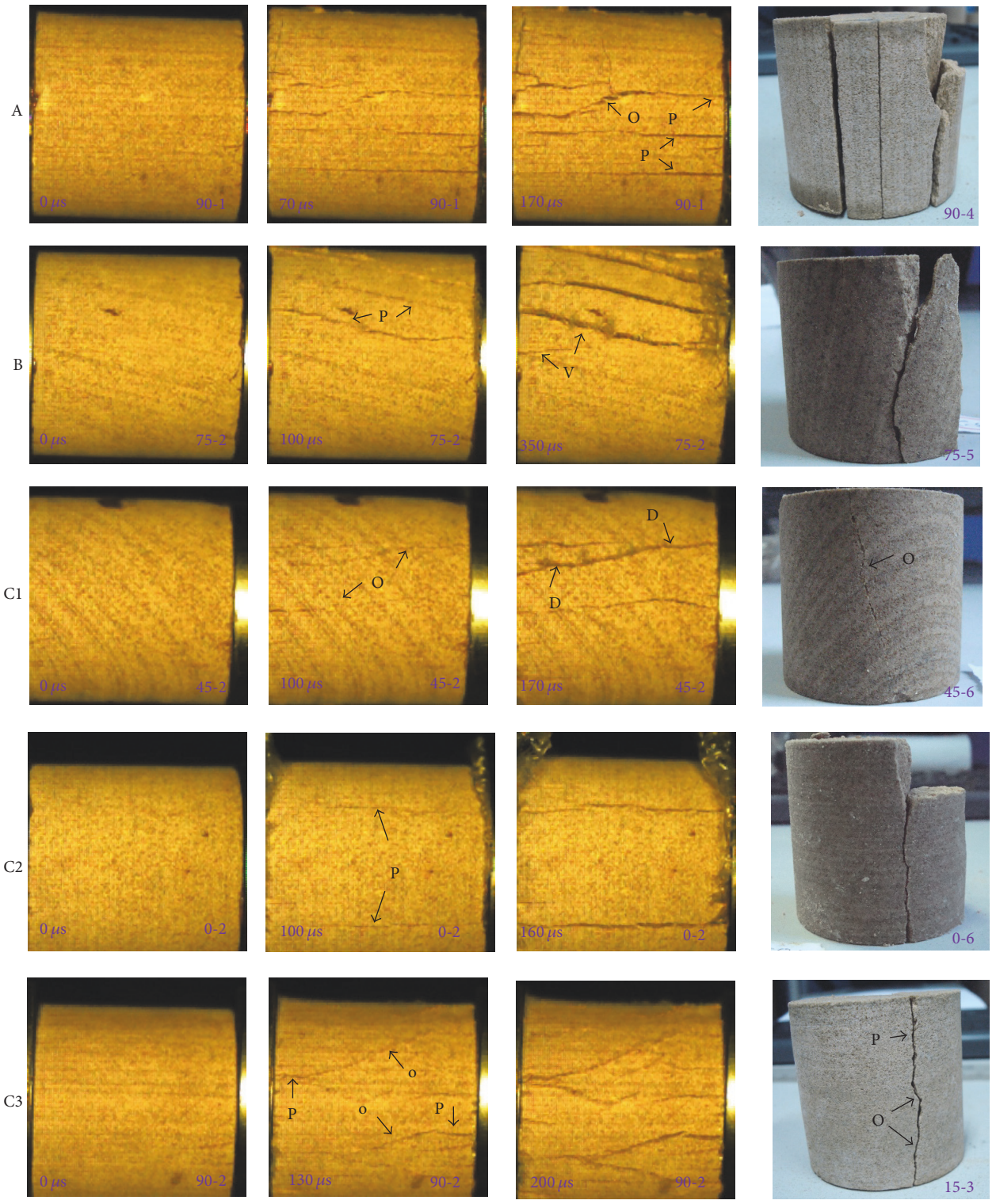

(a) Typical fracturing process

(b) Typical failure

Figure 2: Typical failure patterns of bedded sandstone specimens under impact loading. (Note: P represents the fractures paralleled to loading direction; O represents the fractures oblique to loading direction; V represents V-shaped fractures zone; D represents tiny dislocation.)

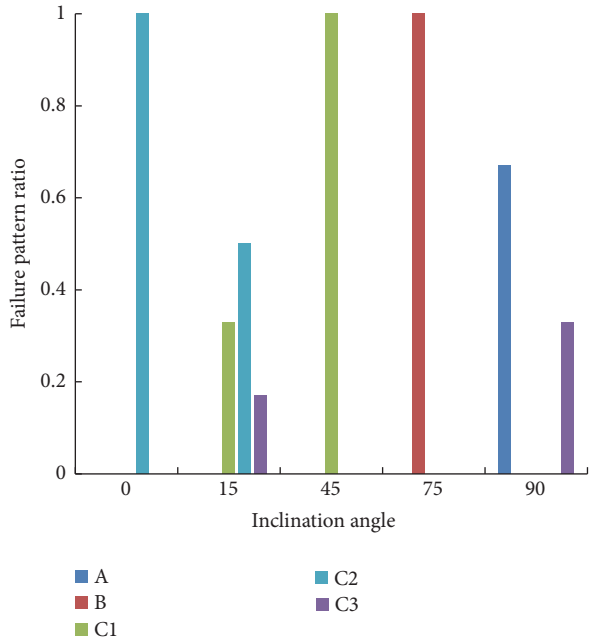

Figure 3: The relationship between failure pattern ratio and inclination angle for bedded sandstones ((A) splitting along bedding planes; (B) sliding failure along bedding planes; (C1) fracturing oblique to loading direction; (C2) fracturing parallel to loading direction; (C3) mixed fracturing across bedding planes.).

the increase of inclination angle. (3) As the inclination angle continues to increase, the failure pattern will change from pattern B to pattern A. When it approaches to 90°, most specimens fail in splitting along bedding planes.

4. Numerical Investigations

Laboratory tests can well reflect the macroscopic deformation behaviors of rock, but they have a shortage in revealing microscopic deformation and fracturing mechanism. From Figure 2, the macroscopic failure patterns have been identified by high-speed camera photograph. In order to further investigate the micro fracturing mechanism, a particle flow code (PFC) numerical model is used to simulate the dynamic failure of layered rock in SHPB test.

4.1. Basic Methodology of PFC

4.1.1. Bonded-Particle Model. The bonded-particle model is represented by a dense packing of nonuniform sized circular particles bonded at their contact points. All particles are bonded together with parallel bond (PB) or contact bond (CB). The two basic bond models have specific force-displacement law. A CB model can provide the behavior of an infinitesimal, linear elastic, and either frictional or bonded interface, which carries a point force and does not resist relative rotation. The PB model provides the force-displacement behavior of a finite-sized piece of cementitious material deposited between two pieces in the vicinity of the contact location, acting in parallel with a linear model; particle can freely move in the shear and normal direction and even rotate between particles. With the PB model, the moment induced by these rotations can be resisted by the bond. With the CB model, however, the moment cannot be resisted. The mechanical behavior of model is governed by Newton's second law of motion and these force-displacement laws. Thus, the micro fracturing process can be simulated as the movement of particles and individual bond breakages [25, 26].

4.1.2. Numerical Model of Transversely Isotropic Rocks in SHPB Test. As shown in Figure 4, the numerical SHPB system was established. All components of SHPB system in experiment were simulated by PFC2D. In order to reduce the amount of calculation, the CB model was assigned on the transmitted bar, incident bar, and striker. Besides, the lengths of transmitted bar and incident bar were set to 0.75 m and 1.5 m. The density of bars particles and striker particles is 7810 kg/m^3, and the contact bond strength was selected to be high enough to avoid damage during the impact test. The previous studies have been revealed that these settings are feasible [27, 28]. Because the impact velocity of striker in laboratory test was 9.4~10.2 m/s, and the impact velocity of analogue striker was set to be 10 m/s.

Cylindrical specimens (7283 particle, 50 mm × 50 mm) were produced, and the particle radius of specimen is in the range of 0.3 mm~0.6 mm. Special particles with radius of 1 mm were aligned to the end of striker, incident bar, specimen, and transmitted bar to improve the contact condition [27]. The features of layered rock were modeled by two steps. Firstly, a simplified numerical model of layered rock was adopted. The particles were divided into two groups to simulate two kinds of rock layers which have different stiffness and strength. The thickness of layers is 10 mm. Most studies have shown that the PB model is more suitable to simulate rock materials than the CB model [26, 29]. Therefore, the particles in analogue specimens are bonded by the PB model. Secondly, the smooth joint (SJ) model was used to simulate the behavior of bedding planes. In previous study, the SJ model has been successfully used to simulate the behavior of bedding planes, joints, foliations, and schistosity [30, 31]. It is suitable for assigning smooth joint model to the interfaces between the two groups of particles. The behavior of a frictional or bonded joint can be modeled by assigning smooth joint models to all contacts between particles that lie on opposite sides of the joint. As shown in Figure 4, it provides the micro behavior of an interface regardless of the local particle contact orientations along the interface. The smooth joint can be envisioned as a set of elastic springs uniformly distributed over a circular cross-section, centered at the contact point and oriented parallel with the joint plane. Once the SJ model is created, preexisting parallel bonds would be deleted and replaced with SJ model. And some parameters such as normal and shear stiffness, tensile, and shear strength need to be reset. The micro parameters of bars, striker, and specimen are listed in Table 1. The elastic bars and striker use the undamped model, in which the damping coefficients were set to zero. And the damping coefficients of analogue layers are set to 0.15. Such

Table 1: Micro parameters of SHPB system and layer rock model.

Analogue object	Density (kg/m^3)	Friction coefficient	Damping	Particle		Bonded model (or SJ model)			
				Normal stiffness	Stiffness ratio (k_n/k_s)	Normal strength/MPa	Shear strength/MPa	Normal stiffness (N/m)	Stiffness ratio ($\overline{k}_n/\overline{k}_s$)
Elastic bars	7810	0	0	6.86×10^{11}	2.8	1×10^{94}	1×10^{94}	—	—
Striker	7810	0	0	6.86×10^{11}	2.8	1×10^{94}	1×10^{94}	—	—
Layer 1	2290	0.58	0.15	8×10^{10}	2	115 ± 10	115 ± 10	8×10^{13}	2
Layer 2	2290	0.58	0.15	6×10^{10}	2	100 ± 15	100 ± 15	6×10^{13}	2
Bedded plane	—	0.58	—	—	—	15	15	2×10^{13}	2

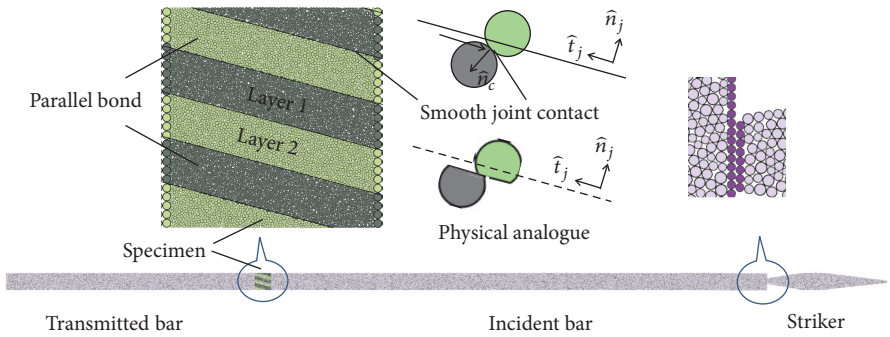

Figure 4: Numerical mode of layered rocks and SHPB system.

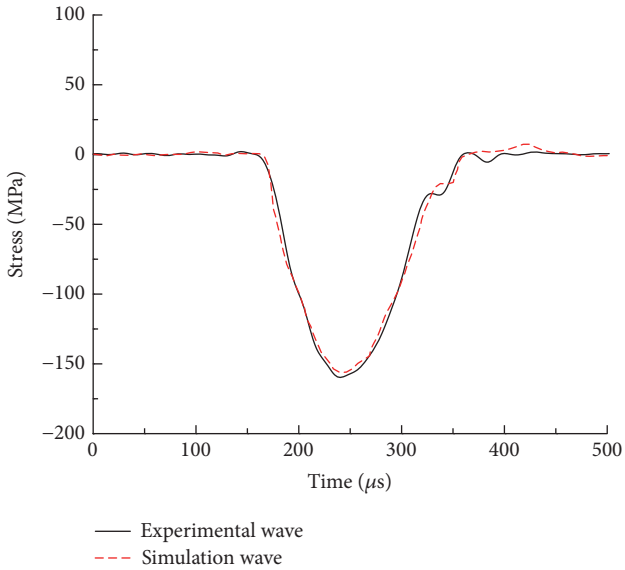

Figure 5: Comparison of incident wave between numerical model and experiment.

arrangements allow the stress wave to propagate effectively, especially the undamped model which ensures that the stress wave propagates through an elastic bar without significant attenuation. Figure 5 shows the comparison of the incident waves obtained by the numerical model and experiment. The good fit between simulation wave and experimental wave ensures the accuracy of the numerical testing.

4.2. Propagation and Evaluation of Micro Cracks. In PFC, once the contact stresses between particles exceed the shear strength or normal strength of the contact, the cracks would be counted and demonstrated. Therefore, the fracturing process of analogue specimen with different inclination angle could be recorded. Besides, the type of cracks is also counted by commands. If the normal tensile stress of a contact exceeds its normal strength, a tensile crack would be registered. Similarly, a shear crack was registered when the shear stress exceeds its shear strength. In addition, the tensile crack and shear crack were further subdivided according to the type of contact. If a PB contact registers a crack, it would be counted as a PB tensile crack or PB shear crack. If a SJ contact registers a crack, it would be counted as a SJ tensile crack or SJ shear crack. The micro cracks of layered rock mode with different inclination angle under impact loading were listed in Table 2.

Figure 6(a) shows the propagation of micro cracks of the analogue specimen with an inclination angle $\theta = 90^\circ$. At the time of 34 μs, some micro cracks begin to develop. Afterwards, the numbers of micro cracks rapidly increase at 52 μs and they are gradually stabilized until 181 μs. The macro failure patterns are similar to the experimental results. It can be seen that the main fractures basically extend along the analogue bedding planes. From the viewpoint of crack number, the SJ tensile cracks and SJ shear cracks contribute to the failure of analogue specimens together (listed in Table 2). And the effect of SJ tensile cracks is slightly larger than that of SJ shear cracks.

Figure 6(b) shows that the analogue bedding planes also play an important role in the fracturing process of the analogue specimen with an inclination angle $\theta = 75^\circ$. The micro cracks initially generate and rapidly increase along the bedding plane at 31 μs. The macro main fractures are composed of SJ shear cracks and SJ tensile cracks, which ultimately penetrated the ends of analogue specimen at 72 μs. Afterwards, some PB cracks including some PB tensile cracks and a few PB shear cracks are generated in analogue rock matrixes due to the action of the subsequent stress wave. Overall, the SJ cracks, especially the SJ shear cracks, dominate the macro fractures of analogue specimen, and then the PB cracks facilitate the analogue specimen to damage further.

Figure 6(c) shows the fracturing process of the analogue specimen with an inclination angle $\theta = 45^\circ$. There are two macro main fractures and some small branching fractures in analogue specimen. One of the macro main fracture is mainly composed of PB tensile cracks and PB shear cracks, which is oblique to the analogue bedding planes. The other macro main fracture is mainly composed of SJ shear cracks and SJ tensile cracks, which extends along the analogue bedding plane. It is different from the experimental results that the analogue bedding planes have actually affected the failure of analogue specimen. There were two features of micro cracks during the fracturing process: (1) both of the SJ cracks and the PB cracks facilitate the analogue specimens to fail. And the action has no obvious stage during the whole of fracturing process; (2) the PB tensile cracks predominate in

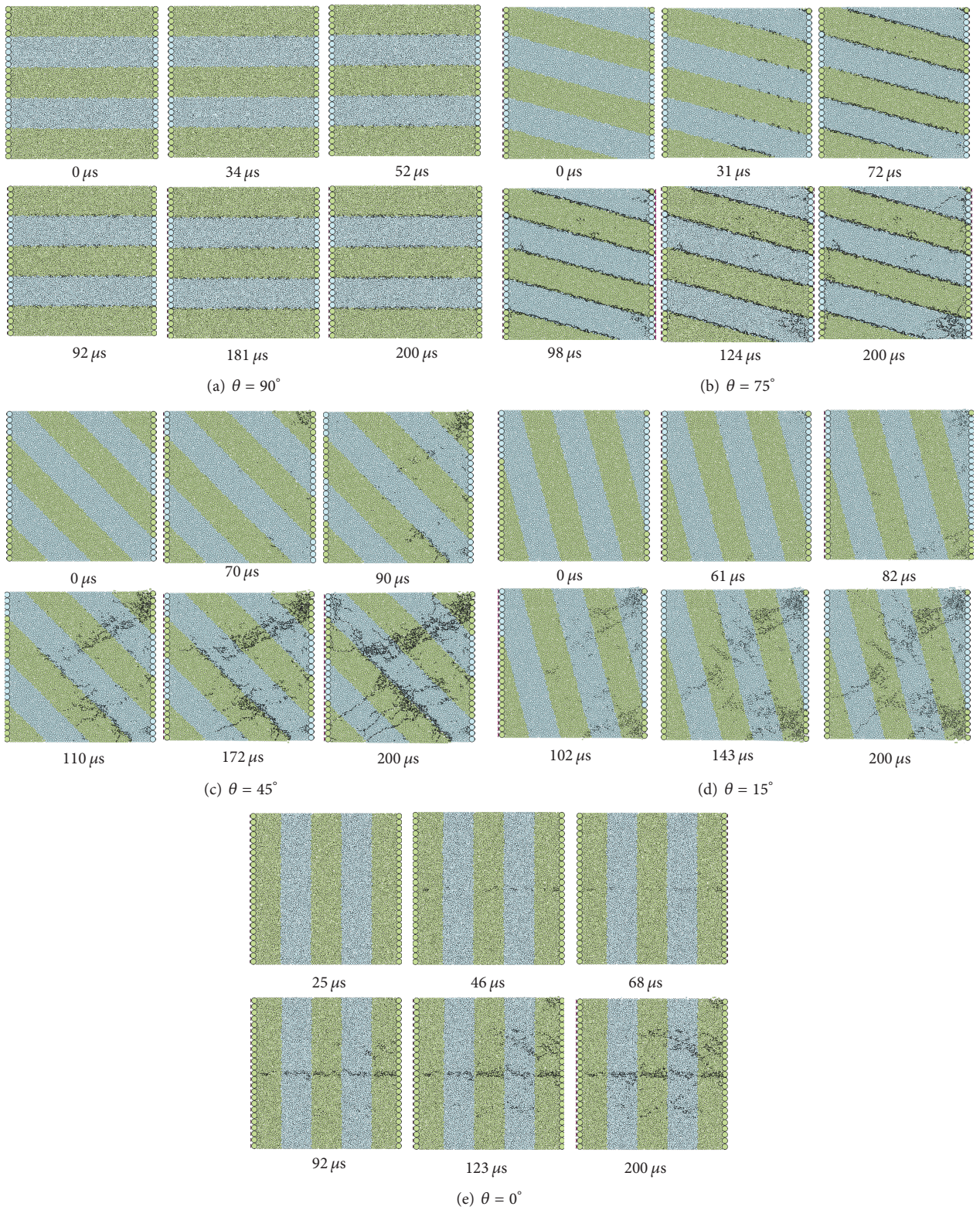

Figure 6: Dynamic fracturing process of layered rock model with different inclination angles.

Table 2: The statistics of micro cracks.

Inclination angle (θ)	PB tensile crack	PB shear crack	SJ tensile crack	SJ shear crack	Total crack
0°	784	149	3	7	943
15°	1750	247	21	100	2118
45°	1992	245	97	354	2668
75°	477	57	355	902	1791
90°	9	2	524	482	1017

the analogue rock matrixes, and the number of PB tensile cracks is more than that of PB shear cracks. The SJ tensile cracks predominate along the analogue bedding planes, and the number of SJ shear cracks is more than that of SJ tensile cracks.

Figure 6(d) shows the fracturing process of the analogue specimen with an inclination angle $\theta = 15^\circ$. It can be seen that the micro cracks are initially generated at 61 μs and ultimately stabilized until 200 μs. The macro main fractures are oblique to the analogue bedding planes. The result agrees well with the experimental phenomenon as shown in Figure 2(C1). Macroscopically, it belongs to the fracturing across bedding planes. The PB tensile cracks predominate the fracturing process. In addition, the SJ cracks are scattered along the analogue bedding planes and these cracks cannot develop to the macro main fracture.

Figure 6(e) shows the propagation of micro cracks of the analogue specimen with an inclination angle $\theta = 0^\circ$. The results show that there are two stages during the fracturing process of analogue specimen. In the first stage, the distributions of most micro cracks are parallel to the loading direction. The micro cracks initially extend toward the ends of analogue specimen before 46 μs and ultimately penetrate the analogue specimen at 92 μs. It is similar to the physical testing results as shown in Figure 2(C2). It belongs to the fracturing parallel to loading direction. In the second stage, many new micro cracks deviate from the location of the macro main fracture. The branching fractures oblique to the loading direction gradually develop and facilitate the analogue specimen to damage further. Figure 7 quantitatively shows the variation of crack number. As shown in Figure 7, the micro cracks emerge at about 25 μs and rapidly increase after 68 μs. The crack numbers are basically stable at about 180 μs. The PB tensile cracks always predominate during the fracturing process.

Overall, the macro failure processes of analogue specimens are similar to the testing results of physical specimens. For the macro main fractures of analogue specimens and physical specimens, the development paths and the geometric relationship with bedding planes are basically the same. Obviously, whether it is experiment or numerical simulation, the bedding planes play an absolute dominant role in the fracturing process at $\theta = 75^\circ$ ~90° and has less effect on the fracturing process at $\theta = 0^\circ$ ~15°. There are also a few differences between experimental results and numerical results: (a) a few branch fractures oblique to bedding planes are occasionally generated in physical specimens at $\theta = 90^\circ$; (b) a macro main fracture along the bedding plane is generated in analogue specimens at $\theta = 45^\circ$. An important

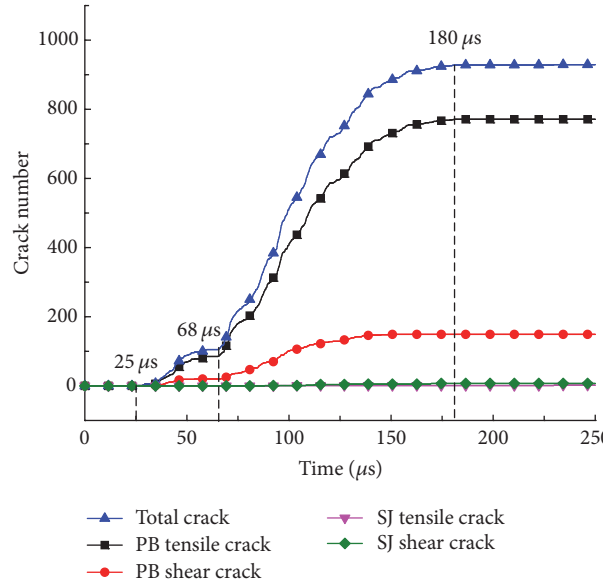

Figure 7: The variation of crack number with time of the analogue specimen ($\theta = 0^\circ$).

reason leading to the difference is that the interlayer spaces of physical specimens are smaller than that of analogue specimens. For the physical specimens, when the cracks propagate along bedding planes, it may be easy to change the propagation direction due to the stress concentration at the tips of cracks. Thus, the influence of bedding planes on the fracturing process of physical specimens is also relatively weaker than that of analogue specimens. Correspondingly, the macro main fractures along the bedding planes has not been observed in physical specimens at $\theta = 45^\circ$, as shown in Figure 2(C1). In general, the numerical simulation results are reliable and agree well with the experiments results. The experimental and the numerical results reveal the dynamic fracturing behavior of layered rock mass effectively from both macro and micro viewpoints.

4.3. Effect of Inclination Angle on Micro Cracks and Macro Failure. Figures 8(a)–8(e) quantitatively show the variation of micro crack number with inclination angle. It can be seen that the number of PB tensile cracks increases when the inclination angle varies from 0° to 45°. When the inclination angle increases from 45° to 90°, the number begins to decrease. The maximum crack number occurs at the inclination angle 45°. The case of PB shear crack is similar to the results of PB tensile crack, but the maximum crack number occurs at the inclination angle 15°. As shown in Figure 8(c), the number

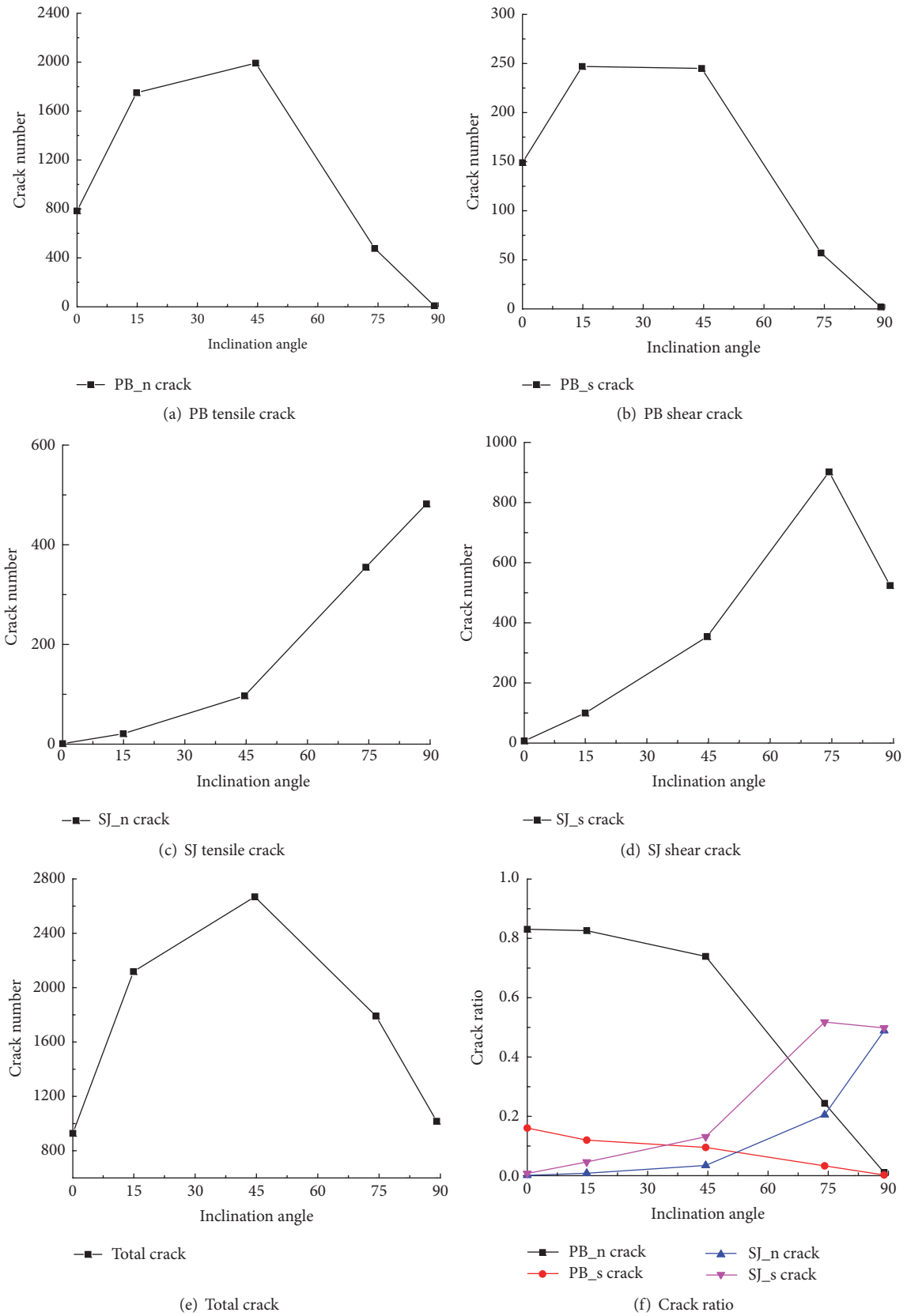

Figure 8: The variation of micro cracks number of analogue layered rock with different inclination angles.

of SJ tensile cracks always increases with the increase of inclination angle. In addition, the number of SJ shear cracks increases at first. When the inclination angle approaches to 90°, the number of SJ shear cracks decreases. The case of total crack is also similar to the results of PB tensile cracks. Generally, the more the number of crack type, the greater the damage caused by that cracks in specimen. Therefore, the above results can reflect the effect of the inclination angle to a certain degree. As shown in Figure 8(f), the ratio of SJ tensile crack and SJ shear crack increases with the increase of inclination angle, which indicates that the greater the inclination angle is, the more the possibility of fracturing along the bedding plane the sample is. On the contrary, the PB cracks decrease with the increase of inclination angle. This shows that the fracturing across the bedding planes is more likely to occur when the inclination angle decreases. Besides, the damage is also more likely to be caused in the rock matrixes rather than along bedding planes. The SJ shear crack is more than the SJ tensile crack when the inclination angle varies from 0° to 75°. This shows that the shear stress is the main reason of the damage along bedding planes at $\theta = 0^\circ \sim 75^\circ$. Similarly, the tensile stress is the main reason of the damage in rock layers at $\theta = 0^\circ \sim 90^\circ$ since the PB tensile cracks are always more than PB shear cracks.

5. Conclusions

Dynamic impact compression tests have been successfully conducted on bedded sandstone specimens. Five groups of specimens with different inclination angles have been tested, including 0°, 15°, 45°, 75°, and 90°. Under dynamic loading condition, failure pattern of bedded sandstone is related to the inclination angle of bedding. Three failure patterns are observed for the impact tests: (A) splitting along bedding planes; (B) sliding failure along bedding planes; (C) fracturing across bedding planes. For the failure pattern (C), three subcategories are also observed: (C1) fracturing oblique to loading direction; (C2) fracturing paralleled to loading direction; (C3) mixed fracturing across bedding planes. For a low inclination angles ($\theta \leqslant 45^\circ$), specimens mainly break across bedding planes, and the occurrence ratio of shear failure will increase with the increase of inclination angle. For a high inclination angles ($\theta \geqslant 75^\circ$), the specimens tend to break along bedding planes.

The numerical mode of SHPB system established by PFC2D reproduces the fracturing process of the layered rock under impact loading. The numerical results show that shear stress is the main reason of the damage along bedding plane at $\theta = 0^\circ \sim 75^\circ$. Tensile stress and shear stress on bedding planes both contribute to the splitting along bedding planes together when inclination angle is 90°. Besides, tensile stress is the main reason of the damage in rock matrixes at $\theta = 0^\circ \sim 90^\circ$.

Conflicts of Interest

The authors declare that they have no conflicts of interest.

Acknowledgments

The authors would like to acknowledge the financial supports from the National Key Basic Research Program of China (no. 2015CB060200), the National Natural Science Foundation of China (Grant no. 51474250), and the Fundamental Research Funds for the Central Universities of Central South University (no. 502221705).

References

[1] Y. Lee and S. Pietruszczak, "Application of critical plane approach to the prediction of strength anisotropy in transversely isotropic rock masses," *International Journal of Rock Mechanics and Mining Sciences*, vol. 45, no. 4, pp. 513–523, 2008.

[2] M. H. B. Nasseri, K. S. Rao, and T. Ramamurthy, "Anisotropic strength and deformation behavior of Himalayan schists," *International Journal of Rock Mechanics and Mining Sciences*, vol. 40, no. 1, pp. 3–23, 2003.

[3] H. Saroglou and G. Tsiambaos, "A modified Hoek-Brown failure criterion for anisotropic intact rock," *International Journal of Rock Mechanics and Mining Sciences*, vol. 45, no. 2, pp. 223–234, 2008.

[4] Y. M. Tien and M. C. Kuo, "A failure criterion for transversely isotropic rocks," *International Journal of Rock Mechanics and Mining Sciences*, vol. 38, no. 3, pp. 399–412, 2001.

[5] W. Wu, G. Jiang, S. Huang, and C. J. Leo, "Vertical dynamic response of pile embedded in layered transversely isotropic soil," *Mathematical Problems in Engineering*, vol. 2014, Article ID 126916, 12 pages, 2014.

[6] J. C. Jaeger, "Shear failure of anistropic rocks," *Geological Magazine*, vol. 97, no. 1, pp. 65–72, 1960.

[7] J. C. Jaeger, N. G. W. Cook, and R. Zimmerman, *Fundamentals of rock mechanics*, John Wiley and Sons, Hoboken, 2009.

[8] X. F. Xian and X. S. Tan, *Failure Mechanism of Layered Rock*, Chongqing university press, Chongqing, China, 1989.

[9] T. Ramamurthy, G. V. Rao, and J. Singh, "A strength criterion for transversely isotropic rocks," in *Proceedings of the Fifth Australia-New Zealand Conference on Geomechanics*, Sydney, Australia, 1988.

[10] O. Saeidi, V. Rasouli, R. G. Vaneghi, R. Gholami, and S. R. Torabi, "A modified failure criterion for transversely isotropic rocks," *Geoscience Frontiers*, vol. 5, no. 2, pp. 215–225, 2014.

[11] Y. M. Tien, M. C. Kuo, and C. H. Juang, "An experimental investigation of the failure mechanism of simulated transversely isotropic rocks," *International Journal of Rock Mechanics and Mining Sciences*, vol. 43, no. 8, pp. 1163–1181, 2006.

[12] D. Q. Dan and H. Konietzky, "Numerical simulations and interpretations of Brazilian tensile tests on transversely isotropic rocks," *International Journal of Rock Mechanics and Mining Sciences*, vol. 71, pp. 53–63, 2014.

[13] X. Tan, H. Konietzky, T. Frühwirt, and D. Q. Dan, "Brazilian tests on transversely isotropic rocks: laboratory testing and numerical simulations," *Rock Mechanics and Rock Engineering*, vol. 48, no. 4, pp. 1341–1351, 2014.

[14] X. B. Li, *Rock Dynamic: Fundmentals and Applications*, Science Press, Beijing, China, 2014.

[15] L. Weng, L. Huang, A. Taheri, and X. Li, "Rockburst characteristics and numerical simulation based on a strain energy density index: A case study of a roadway in Linglong gold mine, China," *Tunnelling and Underground Space Technology*, vol. 69, pp. 223–232, 2017.

[16] J. C. Li, H. B. Li, and J. Zhao, "An improved equivalent viscoelastic medium method for wave propagation across layered rock

masses," *International Journal of Rock Mechanics and Mining Sciences*, vol. 73, pp. 62–69, 2015.

[17] J. B. Zhu and J. Zhao, "Obliquely incident wave propagation across rock joints with virtual wave source method," *Journal of Applied Geophysics*, vol. 88, pp. 23–30, 2013.

[18] X. Liu, F. Dai, R. Zhang, and J. Liu, "Static and dynamic uniaxial compression tests on coal rock considering the bedding directivity," *Environmental Earth Sciences*, vol. 73, no. 10, pp. 5933–5949, 2015.

[19] N. Li, W. L. Chen, and P. Zhang, "Deformation properties of jointed rock mass under dynamic cyclic loading," *Chinese Journal of Rock Mechanics and Engineering*, vol. 20, no. 1, pp. 74–78, 2001.

[20] P. Jia and W.-C. Zhu, "Dynamic-static coupling analysis on rockburst mechanism in jointed rock mass," *Journal of Central South University*, vol. 19, no. 11, pp. 3285–3290, 2012.

[21] A. Fakhimi, F. Carvalho, T. Ishida, and J. F. Labuz, "Simulation of failure around a circular opening in rock," *International Journal of Rock Mechanics and Mining Sciences*, vol. 39, no. 4, pp. 507–515, 2002.

[22] Y. Wang and F. Tonon, "Modeling Lac du Bonnet granite using a discrete element model," *International Journal of Rock Mechanics and Mining Sciences*, vol. 46, no. 7, pp. 1124–1135, 2009.

[23] X. Li, T. Zhou, D. Li, and Z. Wang, "Experimental and numerical investigations on feasibility and validity of prismatic rock specimen in SHPB," *Shock and Vibration*, vol. 2016, Article ID 7198980, 13 pages, 2016.

[24] Z. Zhou, X. Li, and X. Yan, "Loading condition for specimen deformation at constant strain rate in shpb test of rocks," *Chinese Journal of Rock Mechanics and Engineering*, vol. 28, no. 12, pp. 2443–2452, 2009.

[25] 2008, Itasca Consulting Group Inc. Pfc2d user's manual, version 4.0. Itasca Consulting Group Inc, Minneapolis.

[26] D. O. Potyondy and P. A. Cundall, "A bonded-particle model for rock," *International Journal of Rock Mechanics and Mining Sciences*, vol. 41, no. 8, pp. 1329–1364, 2004.

[27] X. Li, Y. Zou, and Z. Zhou, "Numerical simulation of the rock SHPB test with a special shape striker based on the discrete element method," *Rock Mechanics and Rock Engineering*, vol. 47, no. 5, pp. 1693–1709, 2014.

[28] Z.-L. ZHOU, Y. ZHAO, Y.-H. JIANG, Y. ZOU, X. CAI, and D.-Y. LI, "Dynamic behavior of rock during its post failure stage in SHPB tests," *Transactions of Nonferrous Metals Society of China*, vol. 27, no. 1, pp. 184–196, 2017.

[29] T. Liu, B. Lin, Q. Zou, C. Zhu, and F. Yan, "Mechanical behaviors and failure processes of precracked specimens under uniaxial compression: A perspective from microscopic displacement patterns," *Tectonophysics*, vol. 672-673, pp. 104–120, 2016.

[30] B. Park and K.-B. Min, "Bonded-particle discrete element modeling of mechanical behavior of transversely isotropic rock," *International Journal of Rock Mechanics and Mining Sciences*, vol. 76, pp. 243–255, 2015.

[31] W. Chu, C. Zhang, and J. Hou, "A particle-based model for studying anisotropic strength and deformation of schist," in *Proceedings of the 3rd ISRM SINOROCK symposium*, pp. 593–596, International Society for Rock Mechanics and Rock Engineering, Shanghai, China, 2013.